

Reviewed Preprint

v1 • May 29, 2026

Not revised

✉ For correspondence:

Nikolaos.Sgourakis@Pennmedicine.upenn.edu

nn.edu

* These authors contributed equally to the work

Competing interests: No competing interests declared

Funding: See page 16

Reviewing editor: Julien Roche, Iowa State University, United States

© 2026, Rotsides et al. This article is distributed under the terms of the [Creative Commons Attribution License](#), which permits unrestricted use and redistribution provided that the original author and source are credited.

A miniaturized MR1 metabolite display system with native-like protein features

Photis Rotsides^{1,2,*}, Omkar Shinde^{1,2,*}, Julia N Danon¹, Nikolaos G Sgourakis^{1,2} ✉

¹Center for Computational and Genomic Medicine, Department of Pathology and Laboratory Medicine, The Children's Hospital of Philadelphia, Philadelphia, United States • ²Department of Biochemistry and Biophysics, Perelman School of Medicine, University of Pennsylvania, Philadelphia, United States

eLife Assessment

The manuscript by Rotsides et al. reports the design and validation of SMART-MR1, a miniaturized MR1 metabolite-display platform in which the α_1/α_2 ligand-binding domain is stabilized by a synthetic helical domain in place of the α_3 domain and β_2 -microglobulin. Supported by biochemical, biophysical, and structural approaches, including ITC, NMR, and cryo-EM, the work provides **solid** evidence that SMART-MR1 retains native-like ligand binding and A-F7 TCR recognition while enabling experimental approaches for ligand screening that are difficult with conventional MR1 constructs. The study is **valuable** for the MR1 and MAIT-cell fields, particularly as a tool for ligand screening and mechanistic studies of MR1-restricted antigen presentation. There are several suggestions to further strengthen the study's impact, including clearer benchmarking against existing MR1 platforms, broader validation across ligands and TCRs, and functional evidence from MAIT-cell staining or activation assays.

<https://doi.org/10.7554/eLife.111511.1.sa3>

Abstract

Major histocompatibility complex class I-related protein 1 (MR1) presents metabolite-derived antigens to mucosal-associated invariant T (MAIT) cells and other MR1-restricted T cells, playing a critical role in immune surveillance during infection and disease. Biochemical and structural studies of MR1 have been limited by the intrinsic instability of the molecule, which requires both ligand binding and association with beta-2-microglobulin (β_2m) for proper folding and stability. Here, we adapt MR1 to the SMART protein platform to generate a minimalistic system for studying MR1 ligand presentation and T cell receptor (TCR) recognition. SMART-MR1 consists of the MR1 α_1/α_2 ligand-binding platform fused to a helical stabilizing domain that functionally replaces the α_3 and β_2m domains, resulting in a truncated protein that preserves the architecture of the antigen-binding groove. We show that SMART-MR1 can be efficiently produced recombinantly and retains the ability to bind chemically diverse classes of MR1 ligands. The reduced size of SMART-MR1 enables amide-based solution NMR experiments, and its simplified structure allows for ligand screening using fluorescence polarization. Importantly, SMART-MR1 maintains binding to the MAIT-derived A-F7 TCR, as confirmed by isothermal titration calorimetry. Finally, cryo-EM structural analysis of SMART-MR1/5-OP-RU bound to A-F7 revealed that ligand presentation and TCR recognition are nearly identical to those observed in native MR1. Together, these results establish SMART-MR1 as a minimal yet native-like system, expanding the experimental toolkit available for studying MR1 interactions and facilitating future efforts aimed at targeting MR1 pathways.

Significance Statement

MR1 is a highly conserved antigen-presenting molecule that enables T cells to detect metabolite signals from microbial infections and host metabolism. Despite its importance in immunity, mechanistic studies of MR1 have been limited by the instability of the native protein. We developed a simplified and stabilized version of MR1 that preserves the ligand-binding platform while eliminating structural elements that complicate biochemical analysis. This minimal system retains native-like antigen presentation and T cell receptor (TCR) recognition, while enabling experimental approaches that are difficult with full-length MR1. By lowering technical barriers to studying MR1–ligand and MR1–TCR interactions, this platform provides a versatile tool for exploring how antigens shape immune responses and for accelerating discovery of therapeutic strategies targeting MR1.

Introduction

On the surface of all nucleated cells, class I major histocompatibility complex (MHC-I) molecules bind and present a repertoire of peptides derived from the endogenous proteome as a means of immune surveillance by CD8 T cells (1). In an analogous process, the non-classical MHC-I-related protein 1 (MR1) displays small molecule ligands derived from the endogenous and exogenous metabolome to Mucosal-associated invariant T (MAIT) cells and MR1-restricted T cells (2). The MR1 processing and presentation pathway begins with the assembly of a nascent MR1 heavy chain with the light chain beta-2 microglobulin (β_2m) in the endoplasmic reticulum (ER) (3). The assembly process is facilitated by dedicated molecular chaperones: tapasin, which is restricted within the ER-resident peptide-loading complex (PLC), and the homologous, PLC-independent TAP-binding protein related (TAPBPR) (4, 5). However, unlike classical MHC-I, MR1 molecules are only transiently expressed at the cell surface and are rapidly internalized (3, 6). Under steady state conditions, nascent MR1 molecules are localized to the ER, vesicular pools, and endocytic compartments (7–9). These empty MR1 molecules are highly unstable and prone to aggregation. Therefore, MR1 folding and metabolite binding are cooperative processes. The availability of robust ligands triggers MR1 to egress out of the ER, and traffic to the cell surface (4, 10). Alternatively, partially folded MR1 can capture ligands on the cell surface or within vesicular pools, endocytic compartments, and phagosomes to orchestrate host responses (11). Finally, MR1 has a cytoplasmic tyrosine-based motif that is recognized by the endocytic adaptor protein 2 (AP2) complex. This interaction controls the kinetics of MR1 internalization from the cell surface, and minimizes recycling to define the duration of metabolite presentation (12). The importance of MR1 for human health is highlighted by the recent discovery that the human herpesviruses HSV-1 and CMV can disrupt MR1 expression through direct inhibition of the physiological ligand loading process (13).

Canonical MR1 ligands are derived from bacterial metabolite synthesis pathways (14, 15). The two prominent classes are lumazine/pyrimidine derivatives of riboflavin/vitamin B2 (16, 17) and pterins derived from folate/vitamin B9 (18, 19). While RL-6,7-DiMe, Ac-6-FP, and 5-OP-RU all upregulate MR1 surface expression, RL-6,7-DiMe and 5-OP-RU are agonists while 6-FP is antagonistic to T cells (14, 20). Other microbial MR1 ligands, such as 7,8-didemethyl-8-hydroxy-5-deazariboflavin (FO), photolumazines, hesperidin and riboflavin, exhibit pleiotropic properties (15). In contrast to the six polymorphic pockets in the peptide binding groove of MHC-I (A-F), the MR1 groove comprises only A' and F' pockets (18, 21). All MR1 ligands characterized to date bind exclusively to the A' pocket rather than the much shallower MR1 F' pocket (20). It has been proposed that the formation of a Schiff base between the conserved K43 buried in the A' pocket and metabolites promotes stable MR1 folding (3, 18). However, several potent metabolites have been identified which associate with MR1 in a non-covalent manner but still upregulate surface expression levels (14, 22, 23). Consistent with this observation, MR1 K43A mutants can still bind ligands, albeit with decreased thermal stabilities (19, 24), suggesting that K43 Schiff base formation may not be the only determinant for MR1 egress out of the ER, and that both covalent and non-

covalent ligands can form stable complexes with MR1. These knowledge gaps preclude a detailed understanding of what defines a physiologically relevant repertoire of ligands from the cellular metabolome (15).

Previous studies aiming to stabilize the MR1 structure for recombinant protein production and ligand screening applications have used either a chimeric approach where human α_1/α_2 platform is coupled to bovine α_3/β_2m domains (hpMR1)(25), or, more recently an “open” MR1 format, with an engineered disulfide bond at the heavy and light chain interface (26). We have recently developed SMART MHC proteins, which consist of a single-chain α_1/α_2 binding groove with the α_3 and β_2m domains replaced by a helical stabilizing domain (27). Here, we leverage the SMART platform to create a stable minimalistic system for studying MR1 *in vitro*. We demonstrate that SMART-MR1 can capture different classes of known ligands and maintains binding to cognate T cell receptors (TCRs), while also offering new avenues for studying MR1 interactions by solution NMR. We also solve the three-dimensional structure of SMART-MR1 in complex with A-F7, illustrating that SMART-MR1 presents ligands and binds to TCRs similarly to native MR1. Our results demonstrate that SMART-MR1 is a miniaturized system with native-like properties, expanding the potential for studying MR1 using standard biochemical and structural techniques.

Results

Design and purification of SMART-MR1

To determine whether MR1 is a suitable candidate for adapting it to the SMART system, we compared the interface formed by β_2m and the α_1/α_2 “platform” between the structures of human metabolite-bound MR1 (PDB 6PUC) and peptide-bound HLA-A*02:01 (A02, PDB 9SKO). Despite sharing limited (43.6%) overall sequence homology, the α_1/α_2 domains of MR1 and A02 bear considerable structural similarity (Fig. 1A). In both structures, the interface is formed by polar and hydrophobic contacts between key β_2m and α_1/α_2 residues that are conserved between A02 and MR1. Specifically, W60 from β_2m is nestled within a hydrophobic pocket formed by the conserved residue pair M98/95 and F8 under the α_1/α_2 β -sheet, and this interaction plays a central role in both structures. The W60 ring forms a hydrogen bond with D122/118 in A02/MR1, further stabilizing the β_2m /heavy chain interface. Indeed, a key tryptophan at the analogous position in the interface was shown to be favorable when screening for different SMART MHC stabilizing domains (27). Additional stabilizing polar contacts are formed between β_2m residues R3 and D53 with the analogous residues R48/46 and G120/116 in A02/MR1. This striking degree of structural similarity of the β_2m /heavy chain interface in MR1 and A02 suggests that the SMART MHC stabilizing domain can also form the necessary contacts required to stabilize the α_1/α_2 MR1 platform. To this end, we generated a SMART-MR1 construct by joining the N-terminus of the MR1 α_1/α_2 domain to the C-terminus of the SMART MHC stabilizing domain via a rigid linker. Using AlphaFold3, we generated a structural model of SMART-MR1 and found that it closely recapitulated the features of the SMART MHC X-ray structure. In this model, the stabilizing domain formed a network of favorable contacts with the MR1 α_1/α_2 platform. Notably W17 of the SMART-MR1 occupied the hydrophobic pocket under the α_1/α_2 β -sheet, playing an equivalent role to W60 from β_2m in the native MR1 structure (Fig. 1B).

We next sought to express and purify SMART-MR1 from *E. coli* lysates. Our previous work has shown that, while SMART MHC can be expressed in soluble, peptide-receptive form, refolding of the same protein in the presence of excess peptide results in enhanced native structural features and improved affinity for cognate T cell receptors (TCRs) (27). These results suggest that refolded SMART proteins confer superior functionality. We therefore chose to refold SMART-MR1 from *E. coli* inclusion bodies using standard procedures (25, 28). Purification of SMART-MR1 refolded in the presence of the covalent ligand 6-FP by size-exclusion chromatography (SEC) resulted in a monodisperse peak at the expected molecular weight (Fig. 1C and SI Appendix, Fig. S1A). To evaluate the quality of the purified SMART-MR1/6-FP complex we compared its thermal stability to full-length hpMR1/6-FP using differential scanning fluorimetry (DSF). The thermal stability of MR1 complexes is highly dependent on the occupancy a ligand within the A' pocket (5), thus MR1 unfolding is coupled with dissociation of the ligand from the protein. The melting temperature

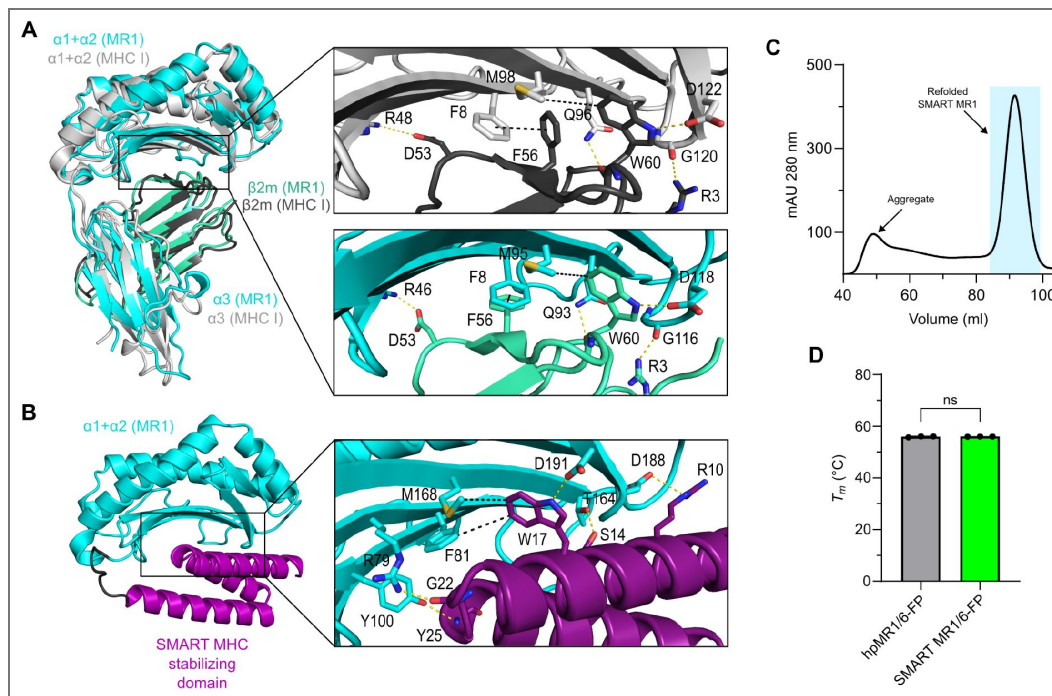


Figure 1. Design and purification of SMART-MR1.

A. Crystal structure of human MR1/ β_2m (PDB 6PUC) superimposed onto the crystal structure of human HLA-A*02:01/ β_2m (PDB 9SKO). Insets illustrate key interactions that stabilize the β_2m interface with the α_1/α_2 domains of HLA-A*02:01/MR1. Polar and hydrophobic contacts are indicated by yellow and black dashes, respectively. **B.** AlphaFold model of SMART-MR1 using the α_1/α_2 domain of MR1 and the stabilizing domain of SMART MHC. The rigid linker connecting the two domains is colored black. **C.** Size exclusion chromatography (SEC) trace of SMART-MR1 refolded in the presence of 6-FP. **D.** Melting temperatures (T_m , °C) obtained from DSF of SMART-MR1 and hpmMR1/ β_2m refolded in the presence of 6-FP. Data are mean \pm s.d. for $n = 3$ technical replicates. Unpaired t-test was performed to obtain a P value of 0.6713, $P > 0.05$ (ns).

(T_m , °C) of SMART-MR1/6-FP was nearly identical to hpMR1/6-FP (56.0 vs 55.9 °C), indicating that SMART-MR1 can bind ligands and present them in a native-like manner (Fig. 1D [↗](#) and *SI Appendix*, Fig. S1B [↗](#)). Together, these results demonstrate that the SMART stabilizing domain can bolster the ligand-binding α_1/α_2 platform of MR1 effectively serving as a functional surrogate of the α_3 and β_2m domains.

Engineered SMART-MR1 can accommodate several classes of known ligands

MR1 is capable of binding to multiple chemically distinct classes of small molecule metabolites. To explore whether SMART-MR1 can capture these diverse ligands, we refolded SMART-MR1 in the absence (empty) or presence of vitamin B9 metabolites (Ac-6-FP, 6-FP), vitamin B2 metabolites (5-OP-RU), and drug or drug-like molecules (3FSA, 5FSA) (Fig. 2A [↗](#)). For all ligands tested, refolding yields improved compared to refolding in the absence of ligand (Fig. 2B [↗](#) and *SI Appendix*, Fig. S2A [↗](#) and C [↗](#)). Moreover, T_m values could only be determined when SMART-MR1 was refolded in the presence of a ligand (Fig. 2C [↗](#) and *SI Appendix*, Fig. S2B [↗](#) and C [↗](#)), likely due to the binding of the hydrophobic dye to the groove of empty SMART-MR1. T_m values also correlated with refolding yields ($R^2 = 0.503$, Fig. 2D [↗](#)). These results indicate that SMART-MR1 binds to different classes of known MR1 ligands, and that, like native MR1, its protein stability is highly dependent upon the presence of bound ligand.

SMART-MR1 is properly conformed and binds the A-F7 TCR with high affinity

To further characterize the structural and biochemical properties of SMART-MR1, and to explore potential applications of our system, we applied solution-based biophysical techniques. A major advantage of SMART-MR1 is that it drastically reduces the size of the complex compared to native MR1 (43 vs 29 kDa). This reduction in size mitigates relaxation losses during NMR experiments, allowing for facile backbone assignments and characterization of interactions with small molecules, immunoreceptors and molecular chaperones, whereas the study of WT MR1 necessitates more elaborate sample preparation with site-selective isotopic labelling (5). To test the feasibility of amide-based NMR experiments, we refolded isotopically labeled SMART-MR1 with 2H , ^{13}C , and ^{15}N in complex with 6-FP, and performed 2D TROSY experiments (Fig. 3A [↗](#)). The 2D TROSY spectrum was well dispersed, as expected for a properly conformed globular protein of 29 kDa, indicating that residue-level information on dynamics and interactions with different binding partners can be obtained using standard solution NMR methods.

We next sought to determine whether SMART-MR1 can be used as a tool to screen for ligand binding. We refolded SMART-MR1 with the non-covalent ligand DCF and used a fluorescent 5-OP-RU analog (JYM20) (4) to perform competition experiments in the presence of a second ligand using fluorescence polarization (FP) (Fig. 3B [↗](#)). Upon incubation of SMART-MR1/DCF with JYM20 for 72 hours at room temperature, we detected an increase in the FP of JYM20 as it transitions into a high MW protein complex. Addition of a competitive ligand (Ac-6-FP) to the sample caused a significant reduction of FP in a dose dependent manner.

Next, we tested binding of SMART-MR1 to an established cognate TCR using isothermal titration calorimetry (ITC) (Fig. 3C [↗](#)). A-F7 is a MAIT cell-derived TCR that specifically binds to MR1 molecules presenting 5-OP-RU. A-F7 binding to SMART-MR1/5-OP-RU was exothermic, driven by a high enthalpy change of -13.5 kcal/mol, and showed a dissociation constant (K_D) of 356 nM, as measured by ITC. This result could suggest an affinity enhancement for SMART-MR1 relative to values reported previously for A-F7 binding to native MR1 (K_D of 1.1 μ M), albeit these experiments were performed using Surface Plasmon Resonance (29). These results demonstrate that SMART-MR1 provides a system for high-resolution solution biophysics by NMR, high-throughput ligand screening, and TCR binding studies.

Figure 2. Ligand dependence of *in vitro* refolding and thermal stability of SMART-MR1 complexes.

A. Chemical structures of ligands tested. **B.** Refolding yields (total mg protein) from SEC purification of SMART-MR1 refolded in the presence of ligands. **C.** T_m values obtained from DSF experiments of SMART-MR1 refolded in the presence of ligands. Data are mean \pm s.d. for $n = 3$ technical replicates. **D.** Correlation plot of T_m versus refolding yield with the coefficient of determination from linear regression (R^2) shown.

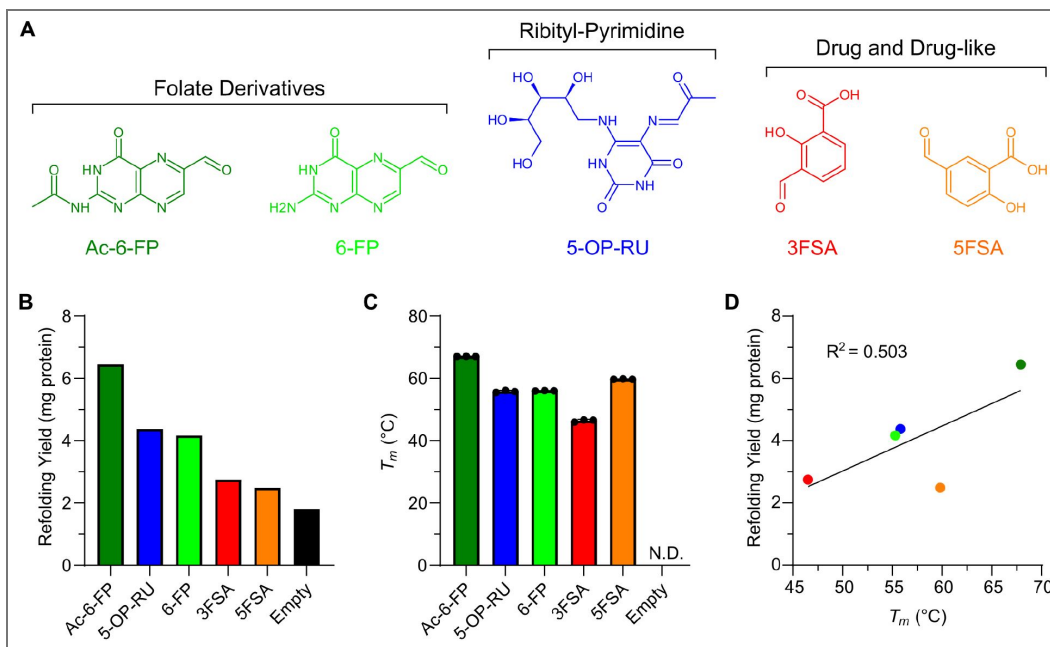
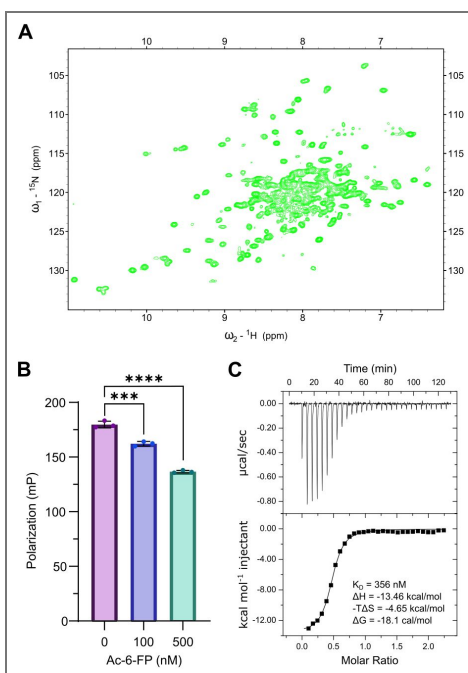


Figure 3. Solution biophysics of SMART-MR1.

A. 2D ^1H - ^{15}N TROSY of 650 μM SMART-MR1/6-FP recorded at a ^1H field of 800 MHz at 25 $^\circ\text{C}$. **B.** Competitive binding of TAMRA-labelled JYM20 to SMART-MR1/DCF as a function of increasing Ac-6-FP concentration, measured by fluorescence polarization. Data are mean \pm s.d. for $n = 3$ technical replicates. One-way ANOVA was performed relative to conditions without Ac-6-FP, $P < 0.0002$ (***) and $P < 0.0001$ (****). **C.** ITC data titrating 200 μM A-F7 TCR into a sample containing 20 μM SMART-MR1/5-OP-RU. Black line is the fit of the isotherm with the K_D and thermodynamic values determined using a 1-site binding model ($n = 1$).



Cryo-EM structure of the SMART-MR1/A-F7 TCR complex reveals a native antigen recognition mechanism

To determine whether SMART-MR1 presents ligands and binds to TCRs in a native-like manner, SEC-purified SMART-MR1/5-OP-RU/A-F7 TCR complex was used to prepare grids for cryogenic electron microscopy (cryo-EM). To overcome the potential preferred orientation issue of the complex during vitrification, 0.01% fluorinated octyl-maltoside was added to the sample prior to grid preparation. Micrographs from cryo-EM data collection revealed an even distribution of particles and 2D classes showed different orientations of the complex. The data processing resulted in a nearly complete cryo-EM map (3.08 Å) of the complex with well-defined densities that allowed unambiguous register of the protein sequence and 5-OP-RU ligand (*SI Appendix*, Fig. S3 and Table S1).

The cryo-EM structure of SMART-MR1 displayed remarkable agreement with the predicted AlphaFold3 model and the native MR1 crystal structure (Fig. 4A). W17 of SMART-MR1 adopts a similar conformation to W60 of β_2m , supporting our prediction that a Trp at this position is key for stabilizing the underside of the MR1 α_1/α_2 domain. We observed a continuous density connecting K116 of SMART-MR1 (analogous to K43 in native MR1) to 5-OP-RU, confirming that SMART-MR1 covalently captures ligands through the formation of a Schiff base (*SI Appendix*, Fig. S4A). The conformation of 5-OP-RU and its interactions within the binding groove remain conserved across the SMART-MR1 and native MR1 structures (Fig. 4B and C). The uracil ring of 5-OP-RU is burrowed within a hydrophobic pocket formed by Y80/W142 and is further stabilized by hydrogen bonds to R82 and S97. The hydroxyl groups of the ribityl chain form a network of polar interactions with R82, R167, Y225, Q226, and W229.

We also observed that the mechanism of 5-OP-RU recognition by A-F7 is nearly identical across the SMART and native MR1 structures. Y95 of the A-F7 complementarity determining region (CDR) 3 α reaches into the MR1 binding groove and forms polar contacts with Y225 and W229 in addition to the ribityl group of 5-OP-RU (Fig. 4D). Furthermore, all six CDR loops of A-F7 dock onto the SMART-MR1 binding groove similarly to native MR1 (Fig. 4E). CDR loops 1 α and 2 α form contacts with the α_1 helix of SMART-MR1, whereas CDR loops 1 β and 2 β interact with the α_2 helix. CDR loops 3 α and 3 β are positioned centrally above the MR1 binding groove, while only CDR3 α is in a favorable position to extend into the A' pocket to make direct contact with the ligand. Together, these structural results demonstrate that SMART-MR1 presents ligands and binds to TCRs in a manner nearly indistinguishable from native MR1.

Discussion

Biochemical characterization of native MR1 presents challenges due to the fact that its stability is coupled to the presence of a ligand within the binding groove, in addition to association with β_2m . Here, we demonstrate that the α_1/α_2 metabolite-presenting platform of MR1 can be stabilized through interactions with a synthetic protein domain, mitigating any concerns caused by β_2m dissociation while maintaining binding to known ligands. Our biophysical data confirm that SMART-MR1 is stable and properly conformed, and that SMART-MR1 binds to cognate TCRs with high affinity. Our structural results demonstrate SMART-MR1 presents ligands in a native-like manner, and that TCRs bind to SMART and native MR1 through identical interactions.

Identifying new ligands and TCRs is critical for understanding MR1 biology in the context of cancer and infectious disease and for developing immunotherapies (22, 29-35). SMART-MR1 provides a platform for rapid exploration of ligand and TCR interactions by various orthogonal techniques. Screening ligands is possible by using SMART-MR1 for high-throughput competitive FP assays. The reduced size and high expression yield of SMART-MR1 allows for mapping of interactions with TCRs by NMR, as illustrated by our recent work using SMART MHC (36). As shown by our current structural determination of the complex with A-F7, SMART MR1 provides an attractive system for high-resolution structural studies of metabolite recognition by MAIT cell receptors using cryo-electron microscopy. Finally, while our work focuses on the MR1*01 allele which has a frequency 71% in humans (37), expanding SMART-MR1 to include less frequent alleles

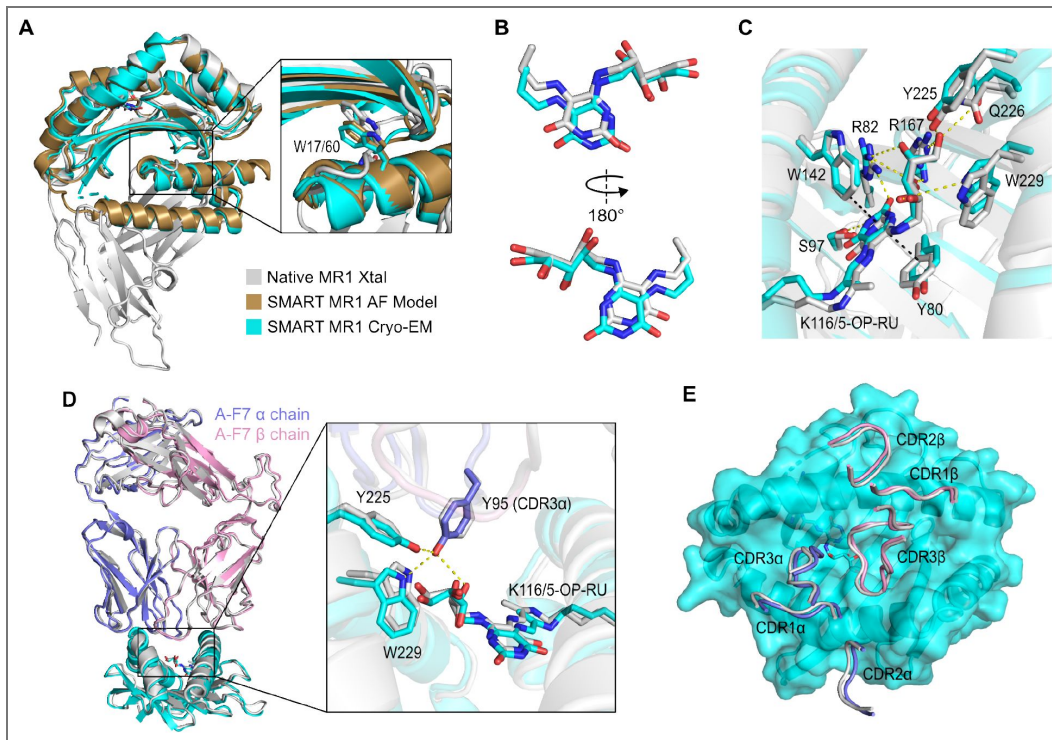


Figure 4. Cryo-EM structure of SMART-MR1/5-OP-RU bound to A-F7 TCR.

A. Cryo-EM structure of SMART-MR1/5-OP-RU superimposed onto the AlphaFold model of SMART-MR1 and the crystal structure of human MR1/h β_2m -5-OP-RU (PDB 6PUC). The inset shows the sidechain of W17 of SMART-MR1 and W60 of h β_2m . **B.** Conformation of 5-OP-RU in the SMART-MR1 Cryo-EM structure superimposed onto 5-OP-RU from the native MR1 crystal structure. **C.** Close up of 5-OP-RU within the ligand binding groove of native and SMART-MR1. Polar and hydrophobic contacts are indicated by yellow and black dashes, respectively. Residues are colored as in panel A. **D.** Cryo-EM structure of A-F7 TCR bound to the α_1/α_2 domain of SMART-MR1/5-OP-RU (cyan) superimposed onto the native MR1/5-OP-RU-A-F7 crystal structure (grey). The inset highlights key interactions between the TCR and the ligand as well as residues within the MR1 groove. **E.** Top view of CDR loop interactions with the surface of SMART-MR1/5-OP-RU. CDR loops are shown as tubes and are colored as in panel D.

can help to determine the effect of polymorphisms on ligand binding and TCR recognition. In summary, SMART-MR1 offers a streamlined and adaptable system that maintains the functional features of MR1, while enabling a wide range of biochemical, structural, and screening approaches for characterizing emerging MR1-restricted antigens relevant to MAIT cell biology, and human disease.

Materials and methods

MR1 ligands

MR1 ligands were purchased from the following suppliers: Ac-6-FP (Cayman Chemical no. 23303), 6-FP (Cayman Chemical no. 14247), 3FSA (3-formylsalicylic acid) (Acros Organics no. 377070250), 5FSA (5-formylsalicylic acid) (Millipore Sigma no. F17601), DCF (Millipore Sigma no. D6899). 5-OP-RU was synthesized in-house from 5-N-RU, which was generously provided by E. Adams (University of Chicago). Chemical structures were prepared using ChemSketch (ACD/Labs).

Protein expression, refolding, and purification

Codon optimized DNA encoding SMART-MR1, hpMR1, or bovine β_2m was transformed into BL21(DE3) *E. coli* (New England Biolabs). Proteins were expressed in autoinducing media at 37 °C overnight (38). Inclusion bodies were isolated and solubilized using guanidine hydrochloride (39). For *in vitro* refolding of SMART-MR1, 60 mg of solubilized inclusion body was slowly diluted into 300 mL of refolding buffer (0.4 M arginine-HCl, 2 mM EDTA, 4.9 mM reduced L-glutathione, 0.57 mM oxidized L-glutathione, 100 mM Tris pH 8.0) at 4 °C while stirring in the absence (empty) or presence of 2 mg of ligand. For hpMR1 refolding, a 50 mg mixture of hpMR1: β_2m at a 1:1 molar ratio was slowly diluted into 1 L of refolding buffer containing 2 mg ligand. Refoldings proceeded at 4 °C for four days without stirring. Solutions were then dialyzed into buffer containing 150 mM NaCl, 25 mM Tris pH 8.0 overnight. The refolding mixtures were concentrated using Pellicon Single-Pass Tangential Flow Filtration (Millipore Sigma) and Amicon ultra centrifugal filters (Millipore Sigma). Purification of refolded MR1 proteins was performed by size-exclusion chromatography using a HiLoad 16/600 Superdex 200 pg column at 1 mL/min in running buffer (150 mM NaCl, 25 mM Tris pH 8.0).

Differential scanning fluorimetry

DSF was used to assess the thermal stabilities of refolded MR1 molecules. 10 μ M protein was mixed with 10 \times SYPRO Orange dye (Invitrogen) in a buffer of 150 mM NaCl and 20 mM sodium phosphate pH 7.4. 20 μ L samples were loaded into MicroAmp Optical 384-well plate and the experiment was performed on a QuantStudio 5 real-time PCR machine with excitation and emission wavelengths set to 470 nm and 569 nm. The temperature was incrementally increased at a rate of 1 °C per minute between 25 and 95 °C. Data analysis and fitting were performed in GraphPad Prism v9.

Nuclear magnetic resonance

To generate isotopically-labeled SMART-MR1, proteins were expressed in M9 media containing 2H_2O , 3 g/L [2H , ^{13}C] glucose, and 1 g/L of $^{15}NH_4Cl$. Protein expression was induced with 1 mM IPTG at $OD_{600}=0.6$ followed by shaking at 37 °C for 5 hours. Inclusion bodies and refolding mixtures were prepared as described above. SEC purification of triple-labeled protein was performed in NMR buffer (100 mM NaCl, 20 mM sodium phosphate, pH 7.2). NMR samples were prepared with 650 μ M protein and 5% 2H_2O . 1H - ^{15}N TROSY HSQC spectra were collected at 800 MHz 1H magnetic field. The data were processed in NMRPipe (40) and analyzed in POKY (41).

Fluorescence polarization

The association of a TAMRA-labeled, fluorescent 5-OP-RU analog (JYM20) (4) to SMART-MR1/DCF was monitored using fluorescence polarization (FP). 10 nM JYM20 was incubated with 10 μ M SMART-MR1/DCF in the absence or presence of increasing amounts of Ac-6-FP for 72 hours at room

temperature in the dark. To determine the optimal incubation conditions for ligand binding, several association assays were performed at room temperature and in 4° C across various incubation times. We found that 48 hours was not sufficiently long enough to facilitate complete association and that at 96 hours a degree of protein degradation had occurred. Additionally, experiments performed at 4° C did not reach full equilibrium, even after 72 hours. Reactions performed at room temperature for 72 hours were able to both reach equilibrium and avoid degradation, a finding consistent across the literature (42). Excitation and emission values used to detect the fluorescence of JYM20 were 531 and 595 nm on a SpectraMax iD5 plate reader. Raw parallel (I_{\parallel}) and perpendicular emission intensities (I_{\perp}) were collected and converted to polarization (mP) values using the equation $1000 * [(I_{\parallel} - G * I_{\perp}) / (I_{\parallel} + G * I_{\perp})]$ with a G-factor of 0.33 for JYM20. The data was analyzed using GraphPad Prism v9.

Isothermal titration calorimetry

ITC was performed using a MicroCal VP-ITC system (Malvern Panalytical, Westborough, MA). All proteins were dialyzed into buffer containing 150 mM NaCl, 25 mM Tris pH 8.0. Syringe containing 200 μ M A-F7 was titrated into a calorimetry cell containing 20 μ M SMART-MR1/5-OP-RU at 25°C. Following an initial 5 μ L injection, injection volumes were 10 μ L for a duration of 20 s and spaced 240 s apart to allow for a complete return to baseline. Data were processed and analyzed with Origin software. Isotherms were fit using a one-site ITC binding model with the first data point excluded from analysis. ITC was performed with one technical replicate.

Cryo-EM sample preparation

The A-F7 TCR/SMART MR1-5-OP-RU complex was purified using SEC and best peak fraction (0.3 mg/mL) was used for grid preparation. Quantifoil R 1/2 300 Mesh, Cu grids were glow discharged at 15 mA for 60s. Prior to the grid preparation, 0.01% fluorinated octyl maltoside was added to the sample to mitigate any preferred-orientation problems. A sample volume of 3 μ L was applied to the grids and subjected to vitrification using a Vitrobot Mark IV system (ThermoFisher) at 4°C with 100 % humidity. The sample was blotted for 3.0 s with a blot force of 2 using Standard Vitrobot 595 filter paper (Ted Pella, Inc) and the grids were plunge-frozen into liquid-nitrogen-cooled liquid ethane.

Cryo-EM data collection, processing, and model building

Cryo grids of the complexes were imaged at 165,000 \times nominal magnification using a Falcon 4 detector (ThermoFisher) on a Glacios 2 (ThermoFisher) microscope operating at 200 kV with a calculated pixel size of 0.6975 Å. Automated image collection was performed using EPU with a nominal defocus range of -0.8 to -2.0 μ m.

For A-F7 TCR/SMART MR1-5-OP-RU complex, 5,448 micrographs were collected using EPU. Data processing was carried out in CryoSPARC v4.7.1. Micrographs were aligned using Patch-motion correction and the Contrast Transfer Function (CTF)-corrected using Patch CTF Estimation in CryoSPARC. Micrographs with CTF fit worse than 10 Å were discarded. Blob picker was used to pick 2,299,717 particles from entire dataset with a minimum particle diameter of 90 Å to a maximum of 180 Å. Particles picked by blob picker were inspected and extracted with a box size of 384 pixels to yield 1,673,666 particles. A round of 2D classification was performed to select best classes (408,724 particles) that look like the desired complex. Ab-initio reconstruction was performed using these particles to get two volumes. One volume containing 248,649 particles was refined to 3.16 Å resolution map. However, this map looked distorted upon rotating by 90° and the density was fragmented in multiple regions. The other volume containing 287,776 particles yielded a nearly complete and less distorted map with 3.08 Å overall resolution, thus used for model building.

For the densities corresponding TCR and MR1 heavy chain, previously solved structure of human MAIT A-F7 TCR in complex with human MR1-5-OP-RU (PDB ID: 6PUC) without α 3 domain and β 2m was used for docking. For the density corresponding to the stabilization domain, bundle consisting

of three N-terminal helices of miniaturized HLA-A*02 (PDB ID: 9NDS) was used for docking. Both models were docked in the cryo-EM density map using UCSF Chimera. The model was manually adjusted in Coot and refined using real-space refinement in PHENIX package.

Data availability

Atomic coordinates for the SMART-MR1/A-F7 TCR complex have been deposited in the PDB under the accession code 10VM.

Supporting information

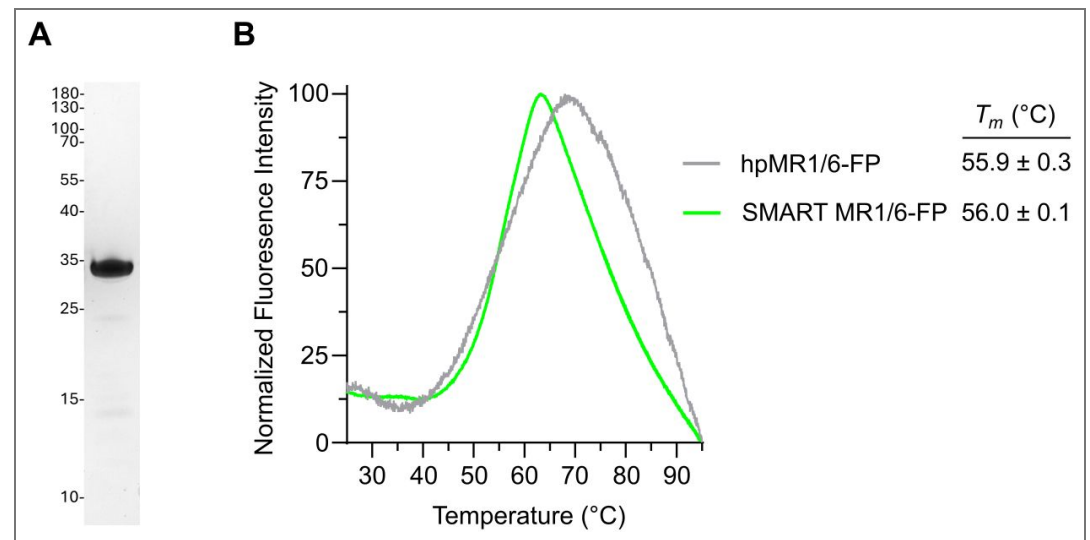


Figure S1. Thermal stability of SMART-MR1 compared to full-length MR1. **A.** SDS-PAGE gel of purified SMART-MR1 refolded with 6-FP. **B.** Normalized DSC traces of purified SMART-MR1 and human platform MR1 (hpMR1) refolded with 6-FP. Data are mean \pm s.d. for $n = 3$ technical replicates.

Figure S2. SEC traces and DSF curves of refolded SMART-MR1 complexes.

A. Size exclusion chromatography (SEC) traces of SMART-MR1 refolded in the absence (empty) and presence of ligand. SEC traces for MR1 are color coded as shown in panel C. **B.** Normalized DSF traces of purified empty and ligand loaded SMART MR1. **C.** Summary of refolding yields obtained from SEC experiments and melting temperatures (T_m) obtained from DSF experiments. Data are mean \pm s.d. for $n = 3$ technical replicates.

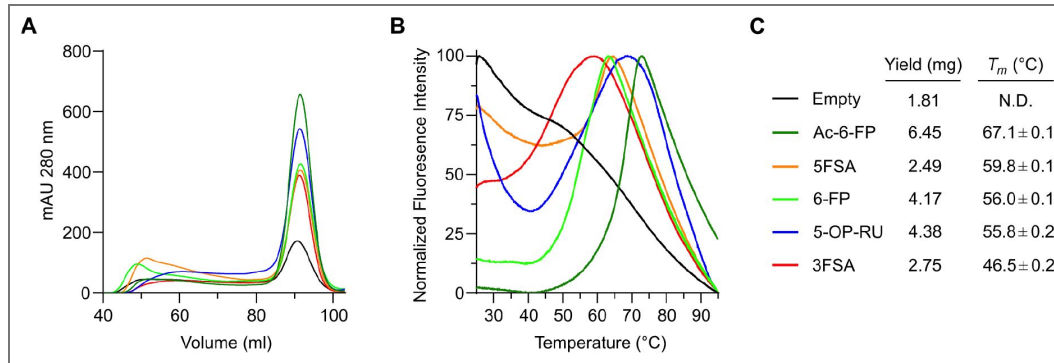
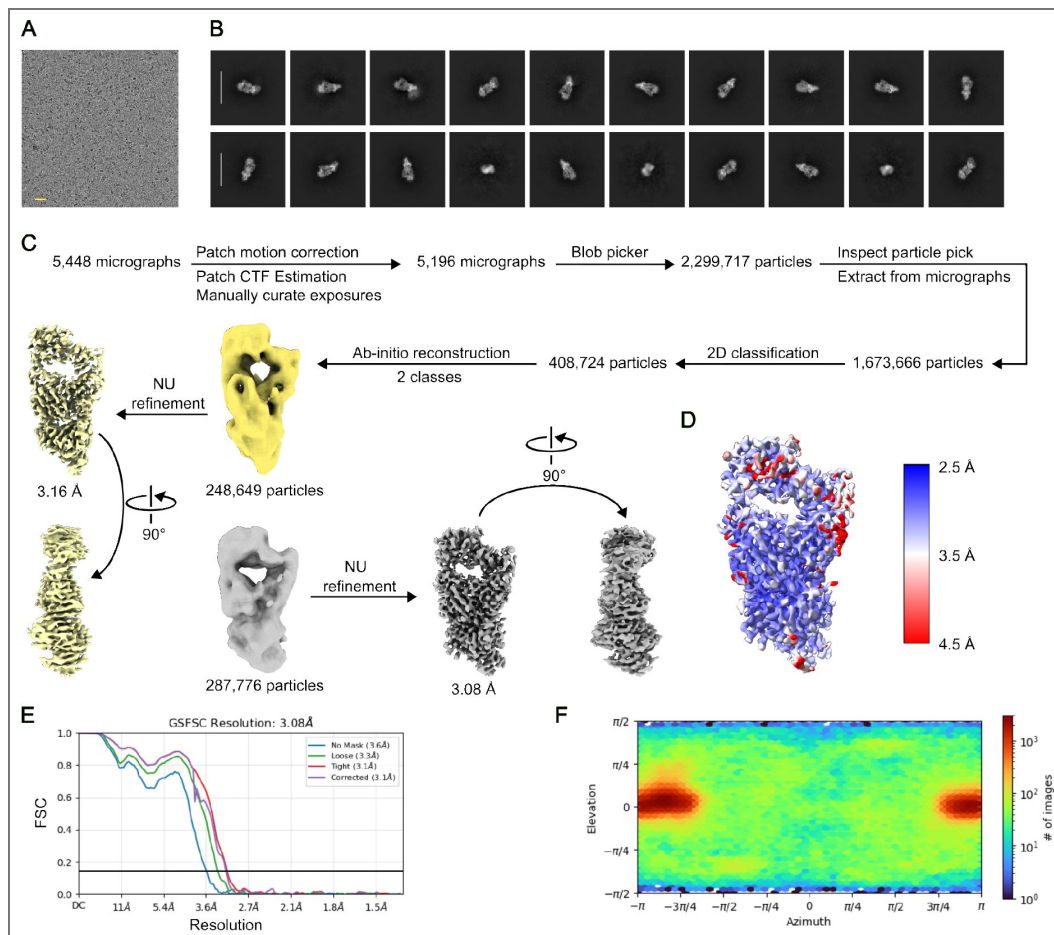


Figure S3. Cryo-EM data processing for A-F7 TCR in complex with SMART-MR1-5-OP-RU.

A. Representative micrograph of the collection for A-F7 TCR/SMART-MR1-5-OP-RU complex. Scale bar in yellow is 200 Å. **B.** Representative 2D classes of A-F7 TCR/SMART-MR1-5-OP-RU complex. Scale bar in white is 150 Å. **C.** Cryo-EM data processing workflow of A-F7 TCR/SMART-MR1-5-OP-RU complex. **D.** Local-resolution estimation of reconstructed map as determined within CryoSPARC. **E.** Gold-standard FSC curves used for global-resolution estimates within CryoSPARC. **F.** Viewing direction distribution of the reconstructed map.



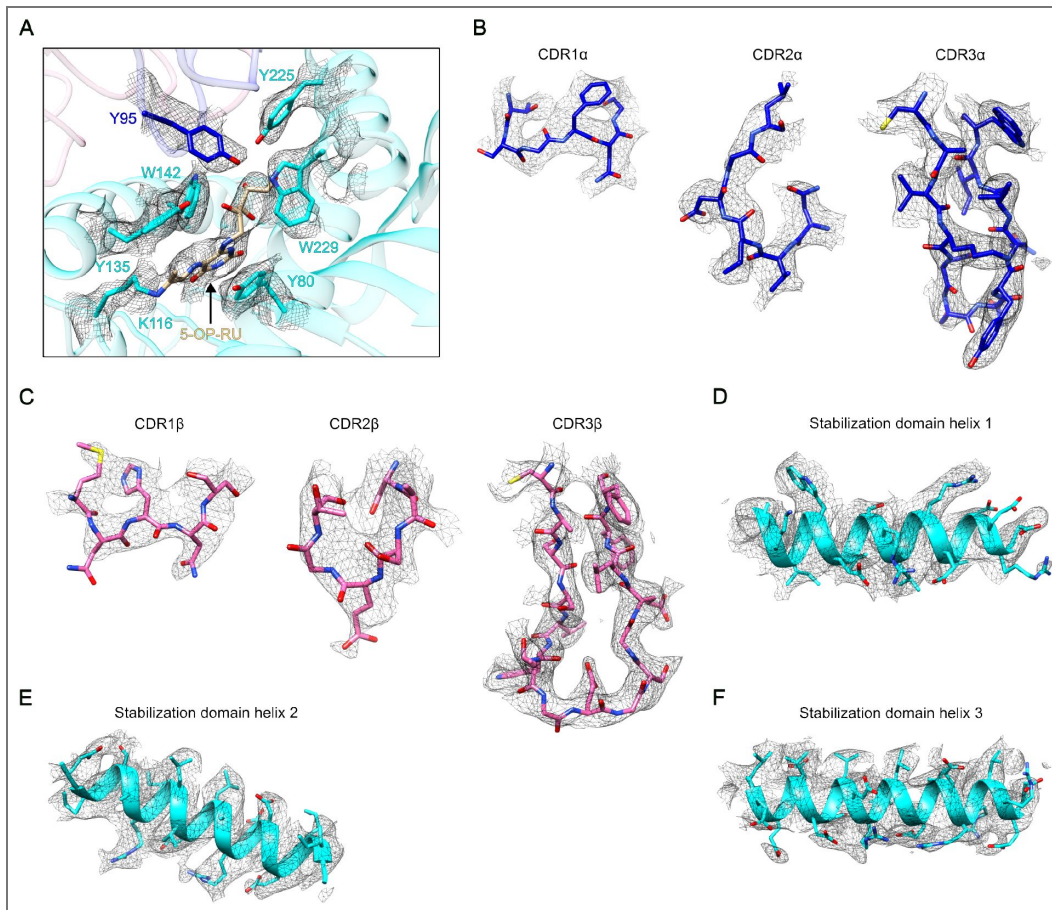


Figure S4. Quality of SMART-MR1-A-F7 cryo-EM map.

A. Cryo-EM density of 5-OP-RU and the residues interacting with it. MHC is colored cyan, TCR α in blue, TCR β in pink, and 5-OP-RU in light brown. Map is contoured at 0.196. **B.** Cryo-EM densities of CDRs of TCR α . Maps are contoured at 0.150 (CDR1 α), 0.200 (CDR2 α), and 0.180 (CDR3 α). **C.** Cryo-EM densities of CDRs of TCR β . Maps are contoured at 0.240 (CDR1 β), 0.140 (CDR2 β), and 0.120 (CDR3 β). **D-F.** Cryo-EM densities of stabilization domain helices. Maps are contoured at 0.095 (D), 0.085 (E), and 0.070 (F).

Human MAIT A-F7 TCR in complex with miniaturized
MR1-5-OP-RU
(EMDB EMD-75491)
(PDB 10VM)

Data collection and processing

Magnification	165,000×
Voltage (kV)	200
Electron exposure (e ⁻ /Å ²)	40
Defocus range (μm)	-0.8 to -2.0
Pixel size (Å)	0.6975
Symmetry imposed	C1
Initial particle images (no.)	2,299,717
Final particle images (no.)	287,776
Map resolution (Å)	3.08
FSC threshold	0.143
Map resolution range (Å)	2.58-3.58

Refinement

Initial model used (PDB code)	6PUC, 9NDS
Model resolution (Å)	3.3
FSC threshold	0.5
Model resolution range (Å)	3.0-3.3
Model composition	
Non-hydrogen atoms	5442
Protein residues	680
Ligands	1
<i>B</i> factors (Å ²)	
Protein (min/max/mean)	14.82/135.30/60.82
Ligand (min/max/mean)	10.56/34.03/23.29
R.m.s. deviations	
Bond lengths (Å)	0.004

Supplementary Table S1. Cryo-EM data collection, refinement and validation statistics SMART-MR1/A-F7 TCR

Bond angles (°)	0.605
Validation	
MolProbity score	2.67
Clashscore	12.55
Poor rotamers (%)	6.07
Ramachandran plot	
Favored (%)	92.56
Allowed (%)	7.44
Disallowed (%)	0.00

Supplementary Table S1. (continued)

Acknowledgements

This work was delivered as part of the MATCHMAKERS Team supported by the Cancer Grand Challenges partnership funded by Cancer Research UK (CGCATF-2023/100004) and the National Cancer Institute (OT2CA297575) and The Mark Foundation for Cancer Research. We acknowledge support by grant NIGMS (7R35GM125034) to N.G.S.

Additional information

Funding

Funder	Grant reference number	Author
Cancer Research UK (CRUK)	CGCATF-2023/100004	Nikolaos Sgourakis
HHS NIH National Cancer Institute (NCI)	OT2CA297575	Nikolaos Sgourakis
HHS NIH National Institute of General Medical Sciences (NIGMS)	7R35GM125034	Nikolaos Sgourakis

Author ORCID iDs

Nikolaos G Sgourakis:  <https://orcid.org/0000-0003-3655-3902>

References

1. Pamer E., Cresswell P. (1998) Mechanisms of MHC class I--restricted antigen processing. *Annu Rev Immunol* **16**:323-358 <https://doi.org/10.1146/annurev.immunol.16.1.323> | PubMed
2. Corbett A. J., Awad W., Wang H., Chen Z. (2020) Antigen Recognition by MR1-Reactive T Cells; MAIT Cells, Metabolites, and Remaining Mysteries. *Front Immunol* **11**:1961 <https://doi.org/10.3389/fimmu.2020.01961> | PubMed
3. McWilliam H. E. G., et al. (2016) The intracellular pathway for the presentation of vitamin B- related antigens by the antigen-presenting molecule MR1. *Nature Immunology* **17**:531-537 <https://doi.org/10.1038/ni.3416> | PubMed
4. McWilliam H. E. G., et al. (2020) Endoplasmic reticulum chaperones stabilize ligand-receptive MR1 molecules for efficient presentation of metabolite antigens. *Proc Natl Acad Sci U S A* **117**:24974-24985 <https://doi.org/10.1073/pnas.2011260117> | PubMed
5. McShan A. C., et al. (2022) TAPBPR employs a ligand-independent docking mechanism to chaperone MR1 molecules. *Nature Chemical Biology* **18**:859-868 <https://doi.org/10.1038/s41589-022-01049-9> | PubMed
6. Gozalbo-López B., et al. (2009) The MHC-related protein 1 (MR1) is expressed by a subpopulation of CD38+, IgA+ cells in the human intestinal mucosa. *Histol Histopathol* **24**:1439-1449 <https://doi.org/10.14670/hh-24.1439> | PubMed
7. Huang S., et al. (2008) MR1 uses an endocytic pathway to activate mucosal-associated invariant T cells. *Journal of Experimental Medicine* **205**:1201-1211 <https://doi.org/10.1084/jem.20072579> | PubMed
8. Harriff M. J., et al. (2016) Endosomal MR1 Trafficking Plays a Key Role in Presentation of Mycobacterium tuberculosis Ligands to MAIT Cells. *PLOS Pathogens* **12**:e1005524 <https://doi.org/10.1371/journal.ppat.1005524> | PubMed
9. Karamooz E., Harriff M. J., Narayanan G. A., Worley A., Lewinsohn D. M. (2019) MR1 recycling and blockade of endosomal trafficking reveal distinguishable antigen presentation pathways between Mycobacterium tuberculosis infection and exogenously delivered antigens. *Scientific Reports* **9**:4797 <https://doi.org/10.1038/s41598-019-41402-y> | PubMed

10. Salio M., et al. (2020) Ligand-dependent downregulation of MR1 cell surface expression. *Proceedings of the National Academy of Sciences* **117**:10465-10475 <https://doi.org/10.1073/pnas.2003136117> | [PubMed](#)
11. Kulicke C. A., et al. (2024) Delivery of loaded MR1 monomer results in efficient ligand exchange to host MR1 and subsequent MR1T cell activation. *Communications Biology* **7**:228 <https://doi.org/10.1038/s42003-024-05912-4> | [PubMed](#)
12. Lim H. J., et al. (2022) A specialized tyrosine-based endocytosis signal in MR1 controls antigen presentation to MAIT cells. *Journal of Cell Biology* **221** <https://doi.org/10.1083/jcb.202110125> | [PubMed](#)
13. Ashley C. L., et al. (2023) Suppression of MR1 by human cytomegalovirus inhibits MAIT cell activation. *Frontiers in Immunology* **14** <https://doi.org/10.3389/fimmu.2023.1107497> | [PubMed](#)
14. McWilliam H. E. G., Villadangos J. A. (2024) MR1 antigen presentation to MAIT cells and other MR1-restricted T cells. *Nature Reviews Immunology* **24**:178-192 <https://doi.org/10.1038/s41577-023-00934-1> | [PubMed](#)
15. Harriff M. J., et al. (2018) MR1 displays the microbial metabolome driving selective MR1-restricted T cell receptor usage. *Science Immunology* **3**:eaao2556 <https://doi.org/10.1126/sciimmunol.aao2556> | [PubMed](#)
16. Eckle S. B. G., et al. (2015) Recognition of Vitamin B Precursors and Byproducts by Mucosal Associated Invariant T Cells*. *Journal of Biological Chemistry* **290**:30204-30211 <https://doi.org/10.1074/jbc.r115.685990> | [PubMed](#)
17. Corbett A. J., et al. (2014) T-cell activation by transitory neo-antigens derived from distinct microbial pathways. *Nature* **509**:361-365 <https://doi.org/10.1038/nature13160> | [PubMed](#)
18. Kjer-Nielsen L., et al. (2012) MR1 presents microbial vitamin B metabolites to MAIT cells. *Nature* **491**:717-723 <https://doi.org/10.1038/nature11605> | [PubMed](#)
19. Eckle S. B. G., et al. (2014) A molecular basis underpinning the T cell receptor heterogeneity of mucosal-associated invariant T cells. *Journal of Experimental Medicine* **211**:1585-1600 <https://doi.org/10.1084/jem.20140484> | [PubMed](#)
20. Awad W., et al. (2020) The molecular basis underpinning the potency and specificity of MAIT cell antigens. *Nature Immunology* **21**:400-411 <https://doi.org/10.1038/s41590-020-0616-6> | [PubMed](#)
21. Huang S., et al. (2005) Evidence for MR1 Antigen Presentation to Mucosal-associated Invariant T Cells *. *Journal of Biological Chemistry* **280**:21183-21193 <https://doi.org/10.1074/jbc.m501087200> | [PubMed](#)
22. Krawic J. R., et al. (2024) Multiple Isomers of Photolumazine V Bind MR1 and Differentially Activate MAIT Cells. *The Journal of Immunology* **212**:933-940 <https://doi.org/10.4049/jimmunol.2300609> | [PubMed](#)
23. Patel O., et al. (2013) Recognition of vitamin B metabolites by mucosal-associated invariant T cells. *Nature Communications* **4**:2142 <https://doi.org/10.1038/ncomms3142> | [PubMed](#)
24. Abdelaal M. R., et al. (2026) The antigen-presenting molecule MR1 binds host-generated riboflavin catabolites. *J Exp Med* **223** <https://doi.org/10.1084/jem.20250711> | [PubMed](#)
25. Ladd N. A., Froyd C. A., Adams E. J. (2020) Production of MR1 Tetramers Loaded with Microbial Ligands. *Methods Mol Biol* **2098**:191-207 https://doi.org/10.1007/978-1-0716-0207-2_13 | [PubMed](#)
26. Sun Y., et al. (2023) Universal open MHC-I molecules for rapid peptide loading and enhanced complex stability across HLA allotypes. *Proceedings of the National Academy of Sciences* **120**:e2304055120 <https://doi.org/10.1073/pnas.2304055120> | [PubMed](#)
27. White W. L., et al. (2026) Design of solubly expressed miniaturized SMART MHCs. *Proceedings of the National Academy of Sciences* **123**:e2505932123 <https://doi.org/10.1073/pnas.2505932123> | [PubMed](#)
28. Garboczi D. N., Hung D. T., Wiley D. C. (1992) HLA-A2-peptide complexes: refolding and crystallization of molecules expressed in *Escherichia coli* and complexed with single antigenic peptides. *Proceedings of the National Academy of Sciences* **89**:3429-3433 <https://doi.org/10.1073/pnas.89.8.3429>

PubMed

29. Chancellor A., et al. (2023) Promiscuous recognition of MR1 drives self-reactive mucosal-associated invariant T cell responses. *Journal of Experimental Medicine* **220** <https://doi.org/10.1084/jem.20221939> | PubMed
30. Vacchini A., et al. (2024) Nucleobase adducts bind MR1 and stimulate MR1-restricted T cells. *Science Immunology* **9**:eadn0126 <https://doi.org/10.1126/sciimmunol.adn0126> | PubMed
31. Protá G., et al. (2025) Mitochondria regulate MR1 protein expression and produce self-metabolites that activate MR1-restricted T cells. *Proceedings of the National Academy of Sciences* **122**:e2418525122 <https://doi.org/10.1073/pnas.2418525122> | PubMed
32. Schmidlin T., et al. (2025) MR1-ligand cross-linking identifies vitamin B6 metabolites as TCR-reactive antigens. *Cell Reports Methods* **5** <https://doi.org/10.1016/j.crmeth.2025.101120> | PubMed
33. Crowther M. D., et al. (2020) Genome-wide CRISPR-Cas9 screening reveals ubiquitous T cell cancer targeting via the monomorphic MHC class I-related protein MR1. *Nature Immunology* **21**:178-185 <https://doi.org/10.1038/s41590-019-0578-8> | PubMed
34. Chengalroyen M. D., et al. (2025) Disruption of riboflavin biosynthesis in mycobacteria establishes riboflavin pathway intermediates as key precursors of MAIT cell agonists. *PLOS Pathogens* **21**:e1012632 <https://doi.org/10.1371/journal.ppat.1012632> | PubMed
35. Jin H., et al. (2022) Deaza-modification of MR1 ligands modulates recognition by MR1-restricted T cells. *Scientific Reports* **12**:22539 <https://doi.org/10.1038/s41598-022-26259-y> | PubMed
36. Woodward C. H., et al. (2025) Solution mapping of MHC-I:TCR interactions using a minimalistic protein system. *Proceedings of the National Academy of Sciences* **122**:e2506016122 <https://doi.org/10.1073/pnas.2506016122> | PubMed
37. Rozemuller E., et al. (2021) MR1 encompasses at least six allele groups with coding region alterations. *Hla* **98**:509-516 <https://doi.org/10.1111/tan.14390> | PubMed
38. Studier F. W. (2005) Protein production by auto-induction in high density shaking cultures. *Protein Expr Purif* **41**:207-234 <https://doi.org/10.1016/j.pep.2005.01.016> | PubMed
39. Li H., Natarajan K., Malchiodi E. L., Margulies D. H., Mariuzza R. A. (1998) Three-dimensional structure of H-2Dd complexed with an immunodominant peptide from human immunodeficiency virus envelope glycoprotein 12011. *Journal of Molecular Biology* **283**:179-191 <https://doi.org/10.1006/jmbi.1998.2091> | PubMed
40. Delaglio F., et al. (1995) NMRPipe: A multidimensional spectral processing system based on UNIX pipes. *Journal of Biomolecular NMR* **6**:277-293 <https://doi.org/10.1007/bf00197809> | PubMed
41. Lee W., Rahimi M., Lee Y., Chiu A. (2021) POKY: a software suite for multidimensional NMR and 3D structure calculation of biomolecules. *Bioinformatics* **37**:3041-3042 <https://doi.org/10.1093/bioinformatics/btab180> | PubMed
42. Wang C. J. H., et al. (2022) Quantitative affinity measurement of small molecule ligand binding to major histocompatibility complex class-I-related protein 1 MR1. *Journal of Biological Chemistry* **298**:102714 <https://doi.org/10.1016/j.jbc.2022.102714> | PubMed

Peer reviews

Reviewer #1 (Public review):

Summary:

This study presents an important tool for the study of MR1 antigen binding, opening new possibilities, and cutting-edge techniques. The evidence supporting the claims of the authors is solid, although including some functional experiments using primary T-cells would also provide a more complete physiologic evaluation. The work will be of interest to T cell immunologists, in general, especially those studying unconventional T cells.

Strengths:

In this study, the authors developed a single-chain MR1-derived protein by exchanging the $\alpha 3$ domain and $\beta 2$ -microglobulin for a helical stabilizing domain that they had previously developed. The aim was to generate a more compact structure that would still fold properly, without the risk of losing $\beta 2$ -microglobulin. This overall more robust structure would facilitate ligand exploration using various cutting-edge biophysical techniques.

The authors successfully demonstrated that their construct folds similarly to native MR1 and retains the ability to bind MAIT TCR in solution, as shown by cryo-EM experiments. Its melting temperature was equivalent to that of the native protein. Importantly, the construct enables the use of differential scanning fluorometry and transverse relaxation-optimized spectroscopy, which represent the main strengths of this work. These approaches should greatly facilitate the screening of additional unknown ligands and enable interaction mapping.

Weaknesses:

One possible area for improvement would be to extend the validation to additional known ligands, particularly weaker binders. Furthermore, although the cryo-EM data are highly convincing, including either MAIT cell staining or MAIT activation assays with the generated construct would provide stronger functional validation of its equivalence to the wild-type protein with respect to ligand-binding properties.

Overall, this work is of great interest to the field, as several groups worldwide are seeking to identify endogenous/tumour-derived MR1 ligands. In addition, some pathogens lacking the capacity to produce 5-OP-RU have been shown to activate MAIT cells, raising the possibility that unknown pathogen-derived ligands may also exist.

<https://doi.org/10.7554/eLife.111511.1.sa2>

Reviewer #2 (Public review):**Summary:**

The authors develop a miniaturized MR1 construct (SMART-MR1) in which the $\alpha 1/\alpha 2$ platform is stabilized by a synthetic domain, and show that it can bind ligands, engage a cognate TCR, and recapitulate native-like recognition by cryo-EM.

Strengths:

The work is well-written, technically strong and carefully executed. The authors combine biochemical, biophysical and structural approaches, including ITC, NMR and cryo-EM, to show that SMART-MR1 behaves in a manner closely resembling native MR1. The reduction in size and the demonstration of solution NMR are clear practical advantages for certain types of mechanistic studies.

Weaknesses:

The main limitation is that the manuscript does not clearly establish a practical advantage over existing MR1 formats, such as single-chain MR1- $\beta 2M$ or previously described stabilized constructs. The comparison is largely framed against native MR1, which risks overstating the problem, and on the basis of the data presented, it is unlikely that other researchers will adopt this system. In addition, the choice of the A-F7 TCR as a validation reagent may overestimate the generality of the approach, as this receptor is known to exhibit relatively broad ligand tolerance, including recognition of MR1 presenting vitamin B6 metabolites (PDB

9CGR) and structurally diverse synthetic ligands. The extent to which SMART-MR1 supports recognition by a broader range of MR1-restricted TCRs is not addressed.

<https://doi.org/10.7554/eLife.111511.1.sa1>

Reviewer #3 (Public review):

Summary:

This manuscript describes the engineering, production and validation of an MR1 variant with enhanced suitability for screening of ligands and biophysical and structural analysis. The authors utilize a previous advance from their laboratory on a classical MHC (HLA-A2) whereby the alpha 3 and b2m domains are replaced by a helical stabilizing domain.

Strengths:

This variant has a smaller molecular weight than the native MR1, can be produced easily through refolding and is thus much more suitable for NMR analysis. The authors provide data demonstrating that many of the parameters typically evaluated in protein biochemistry/biophysics are similar to reported values between this engineered variant and the wild-type protein. Overall, this is a significant advance to the MR1 field and more broadly to MR1 relevance in immunology and cancer biology, as this will accelerate high-throughput screening and discovery of disease-relevant ligands for MR1, which have been overshadowed by the misguided fixation on 5-OP-RU.

Weaknesses:

Minor concerns about the lack of comparison with the native MR1 extracellular domain construct in the validation of this engineered construct.

<https://doi.org/10.7554/eLife.111511.1.sa0>